Powder Technology 329 (2018) 401–408

Contents lists available at ScienceDirect

Powder Technology

journal homepage: www.elsevier.com/locate/powtec

Preparation and formation mechanism of monodisperse micaceous iron oxide from iron chromium grinding waste

Bo Liu [a], Shen-gen Zhang [a,*], Chein-chi Chang [b], Alex A. Volinsky [c]

[a] Institute for Advanced Materials and Technology, University of Science and Technology Beijing, Beijing, 100083, PR China
[b] Department of Engineering and Technical Services, District of Columbia Water and Sewer Authority, Washington, DC 20032, USA
[c] Department of Mechanical Engineering, University of South Florida, Tampa, FL 33620, USA

ARTICLE INFO

Article history:
Received 1 June 2017
Received in revised form 29 January 2018
Accepted 30 January 2018
Available online 5 February 2018

Keywords:
Micaceous iron oxide
Iron chromium grinding waste
Hydrothermal process
Formation mechanism
Recycling

ABSTRACT

The aim of this study is to develop a new method for the preparation of high-value, environmentally friendly products from iron chromium grinding waste (ICGW). Using iron chromium hydroxide precursors from the wet treatment of ICGW as raw material, monodisperse micaceous iron oxide (MIO) has been prepared via hydrothermal method. The effect of NaOH concentration and hydrothermal reaction temperature on the formation and morphology of obtained MIO powders were investigated carefully. Synthesized MIO powders have high purity (97.6%), even distribution of sizes (~15 μm) and uniform flake. Quality test results showed that MIO products met the first rank criterion of ISO 10601-2007 (the standards of MIO pigments for paints). Furthermore, the formation mechanism of MIO from iron chromium hydroxide precursors was discussed.

1. Introduction

Iron oxide is an important inorganic nonmetallic material, which is widely used in pigments [1,2], catalyzer [3,4], biomedical engineering [5] and other fields [6]. Micaceous iron oxide (MIO), a type of hematite (Fe_2O_3), has attracted much attention due to its good durability, excellent chemical stability and low cost [7–9]. Moreover, MIO has been widely used as the source of magnetic materials and protective coatings, particularly in anticorrosive media in industrial anticorrosion coatings [10–14]. The conventional method to obtain this material is exploitation of the specularite [15], but obtaining monodisperse, high purity and uniform flake powders may not be easy. In order to improve the quality of MIO, numerous synthetic routes have been developed, including high temperature molten salt [16], vapor phase [17], hydrothermal method [18], etc. Compared with other routes, hydrothermal method is of the advantages of less energy consumption, easily-controlled operating condition, good for large-scale serial production and available wastes as raw materials [19,20]. With mineral resources exhaustion and the growing demand for high quality MIO, the hydrothermal synthesis of MIO has been concerned and developed widely in recent years [21,22].

Iron chromium grinding waste (ICGW) is an iron chromium solid waste, resulting from grinding processes of chromium steel. In China, >10 million tons of ICGW are produced each year. The solid waste is a mixture of small metal particles, lubricants, resin adhesive and residuals from grinding media, such as abrasive belts or stone wheels [23]. Due to high impurity content and the strong binding force between the impurities and metal particles, widely used extraction methods of magnetic separation or flotation are ineffective. Chemical treatments have been demonstrated to be effective for iron recovery from refractory wastes [24,25]. However, for ICGW, this processing can generate a large number of chromium laden sludge, instead of highly pure iron oxide or hydroxide. At present, most of ICGW are landfilled or directly re-used in sintering, which can lead to secondary pollution and resource waste. Therefore, technologies for ICGW treatment and reutilization are in urgent demand.

MIO has high economic value and large market demand. If MIO can be synthesized from ICGW, it can be benefited in economy, environment and social. To the best of the author's knowledge, no similar studies have been reported in the literature. Thus, the aim of this study is to report the synthesis of MIO from ICGW via hydrothermal method. The effect of sodium hydroxide (NaOH) concentration and hydrothermal temperature on the formation and morphology of MIO were studied. Furthermore, the formation mechanism of MIO from iron chromium hydroxide precursors was discussed.

* Corresponding author.
E-mail address: zhangshengen@mater.ustb.edu.cn (S. Zhang).

https://doi.org/10.1016/j.powtec.2018.01.085
0032-5910/

Fig. 1. Physical photo of ICGW.

Table 1
Chemical composition (wt%) of the ICGW dried by air.

Components	wt%	Components	wt%
Fe	82.92	Cr	2.00
Mn	0.18	V	0.02
Oil	3.20	Other	13.20

2. Experimental

2.1. Materials and reagents

All reagents used in this study were of analytical grade and locally procured. ICGW samples used in this study were obtained from a Chinese cold rolling production company. Physical photo of ICGW is shown in Fig. 1, from which can be seen that ICGW is dark gray and cotton-like. Table 1 lists the chemical composition of ICGW dried at room temperature. From Table 1, ICGW sample contains predominantly Fe (82.92 wt%), Cr (2.00 wt%), oil (3.20 wt%), small amounts of Mn (0.26 wt%) and V (0.02 wt%).

2.2. Preparation of the MIO pigment

The experimental flow chart is shown in Fig. 2. First, ICGW was weighed (100 g), and leached by 500 mL sulfuric acid (8 mol/L) at 80 °C for 4 h. Then pickling was filtered out and collected. An appropriate amount of hydrogen peroxide (30 wt%) was added to the filtrate so that all iron could exist in the Fe^{3+} form. Subsequently, ammonia, used as precipitant, was dropped into the oxidized solution under continuous stirring until pH reached to about 7.5. As a result, Fe and Cr were precipitated into iron chromium hydroxide precursors ($Fe(OH)_3$ and $Cr(OH)_3$). After filtration, the obtained $(NH_4)_2SO_4$ solution can be used to prepare ammonia by ammonia recycling process. The obtained iron chromium hydroxide precursors were mixed into NaOH solution of certain concentrations (heated to 60 °C in water bath) at a solid to liquid ratio of 1:12. Subsequently, the whole mixture was stirred for 15 min before it was transferred into a Teflon-lined stainless steel autoclave, sealed, and maintained at a certain temperature for 5 h with fill factor 70%. After the heat treatment, the autoclave was cooled to room temperature. Products were obtained and collected by centrifugation separation, and then cleaned ultrasonically several times with deionized water. The liquid from centrifugal separation contained a large amount of NaOH. Therefore, it can be collected and reused.

2.3. Characterization

Soak the ICGW overnight in a large amount of acetone. Then, the ICGW was washed with water, and dried in argon atmosphere. In the above process, the weight loss rate of the ICWG was considered to be the content of oil. Besides, in order to test the content of metal elements in the ICWG, ICWG was digested and analyzed by Inductively Coupled Plasma Optical Emission Spectrometer (ICP-OES, OPTIMA 7000DV, PerkinElmer, USA).

The matter volatile at 105 °C, matter solubility in water, oil absorption value and pH of aqueous suspension of MIO were tested according to general methods of test for pigments and extenders specified by ISO 787-2,3,5,9 [26–29], and the residue on sieve of MIO was tested according to ISO 3549 [30]. Acid dissolution followed by chemical titration was used to determine the content of iron oxide and ferrous oxide of prepared MIO samples.

The X-ray photoelectron spectroscopy (XPS) analyses were performed using AXIS Ultra XPS system (Kratos Analytical, Manchester, United Kingdom) equipped with a Monochromated Al Kα (150 W) as an X-ray source. X-ray powder diffraction (XRD) patterns were recorded using Philips APD-10 X-ray diffractometer with Cu Kα radiation. The morphology of products was observed in the field-emission scanning electron microscope (ZEISS ULTRA 55, Germany). The distribution of elements in the sample was characterized by scanning electron microscopy (ZEISS EVO 18, Germany) coupled with energy dispersive X-ray spectroscopy (EDS).

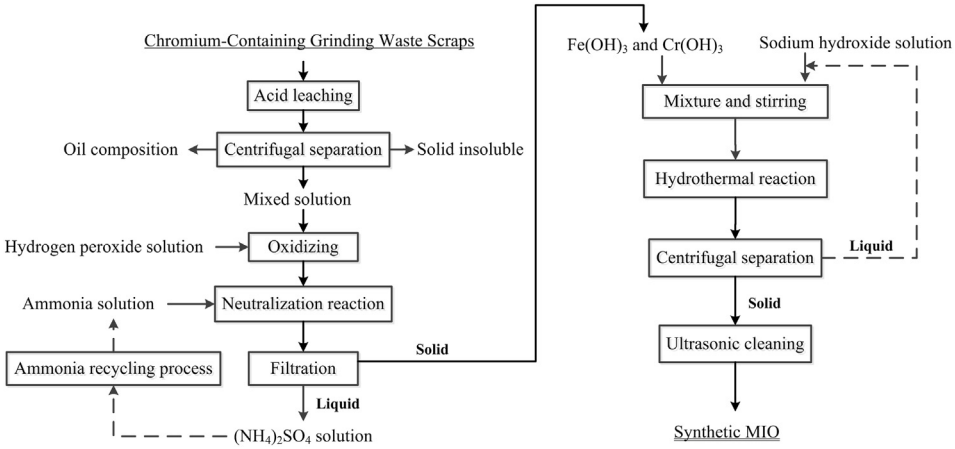

Fig. 2. Preparation flow chart of MIO synthesized from the ICGW.

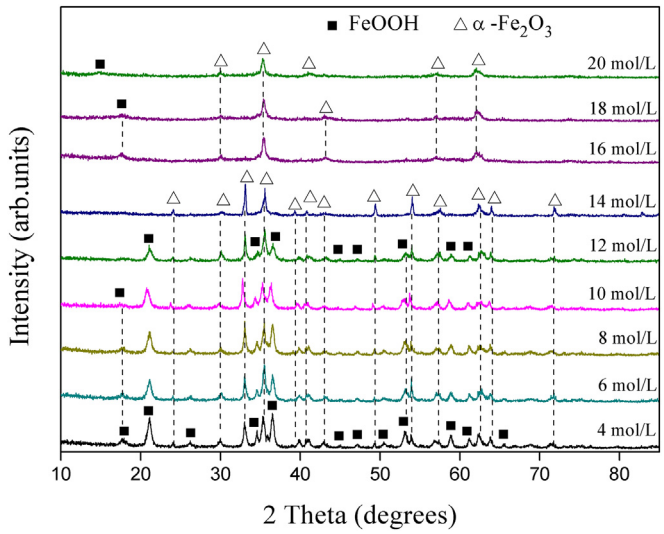

Fig. 3. XRD patterns of MIO prepared at different NaOH concentrations.

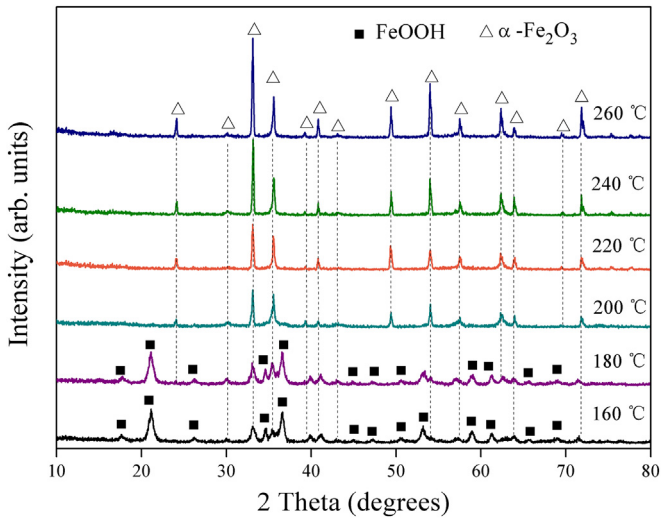

Fig. 5. XRD patterns of MIO prepared at different hydrothermal temperatures.

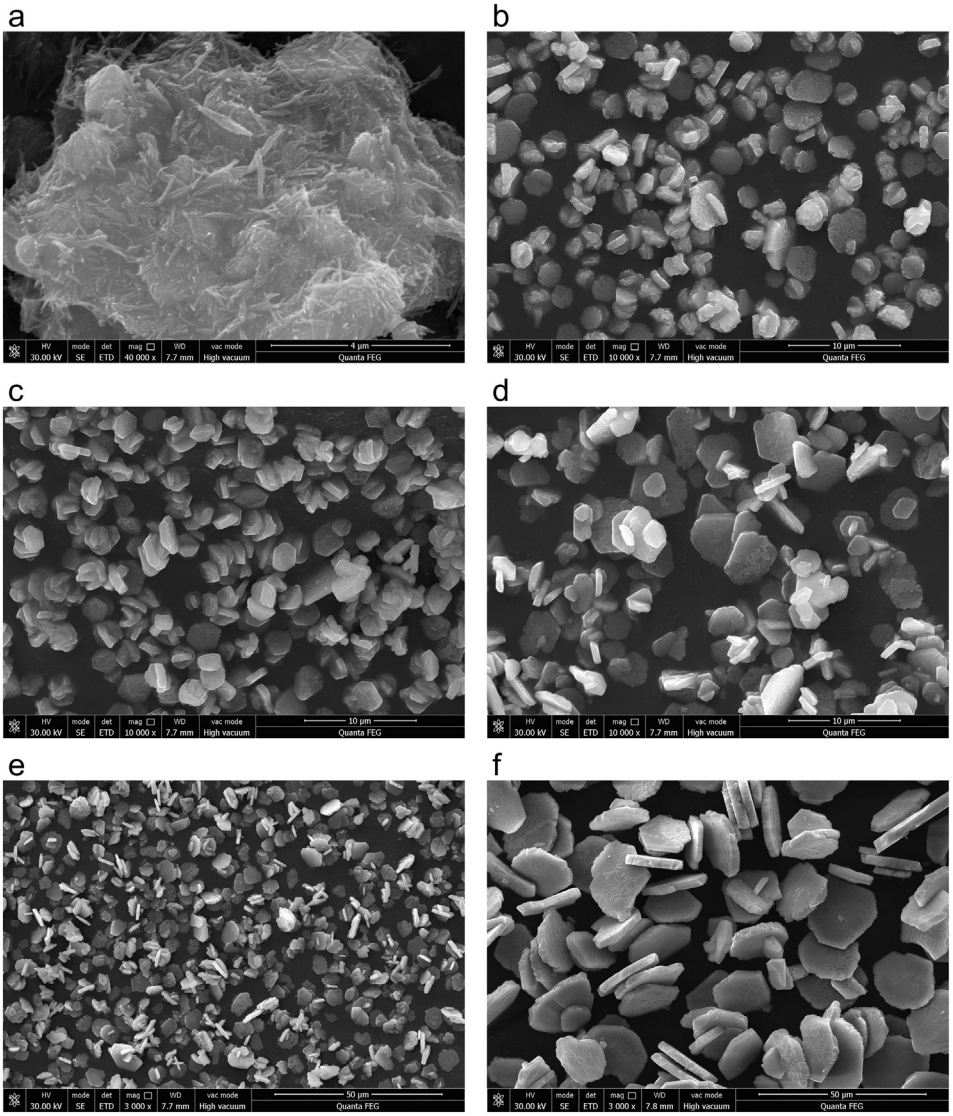

Fig. 4. SEM images of MIO synthesized at different NaOH concentrations: (a) 4 mol/L; (b) 6 mol/L; (c) 8 mol/L; (d) 10 mol/L; (e) 12 mol/L; (f) 14 mol/L.

Table 2
Effect of hydrothermal temperature on the formation and crystalline size of MIO.

Hydrothermal temperature (°C)	% phase obtained	Crystalline size (nm)
160	9.8% α-Fe_2O_3	131
	91.2% FeOOH	313
180	27.3% α-Fe_2O_3	231
	72.7% FeOOH	663
200	98.2% α-Fe_2O_3	424
220	98.3% α-Fe_2O_3	437
240	98.6% α-Fe_2O_3	570
260	98.8% α-Fe_2O_3	610

3. Results and discussions

3.1. NaOH concentration

For the hydrothermal synthesis of MIO from ferric hydroxide precursor, studies have shown that NaOH concentration and reaction temperature are two of the most important influence factors [21,31]. Only when these two factors meet certain conditions, high-quality MIO can be obtained. According to Zheng's point [21], the optimum NaOH concentration should be >7 mol/L, and the optimum reaction temperature should be >200 °C. In our previous studies [31], the optimal conditions were NaOH concentration of 8 mol/L and reaction temperature of 200 °C. Based on these findings, in this study, the two factors were investigated one by one by keeping the other factor constant. Furthermore, the basic values of these two factors were set to 8 mol/L and 200 °C, respectively.

A series of experiments were performed with NaOH concentration ranging from 4 to 20 mol/L, while hydrothermal temperature was fixed at 200 °C. XRD patterns of the as-synthesized products were shown in Fig. 3. The XRD patterns of the 4 mol/L sample showed the presence of FeOOH (JCPDS: 33-0664) and traces of α-Fe_2O_3 phases (JCPDS: 33-0664), which indicated that the reaction from ferric hydroxide precursor to α-Fe_2O_3 is inadequate. As NaOH concentration increased, the content of α-Fe_2O_3 phase increased, and FeOOH phase decreased accordingly. This may be due to the increase of the solubility of FeOOH with increasing NaOH concentration [32–34]. At 14 mol/L, a well-crystallized pure α-Fe_2O_3 phase was formed. However, over 14 mol/L, the sample exhibited more fuzzy diffraction peaks and lower diffraction intensity. Moreover, the presence of FeOOH phases in samples could be observed again. It has been reported that sodium ferrate can be synthesized by the reaction of sodium carbonate and

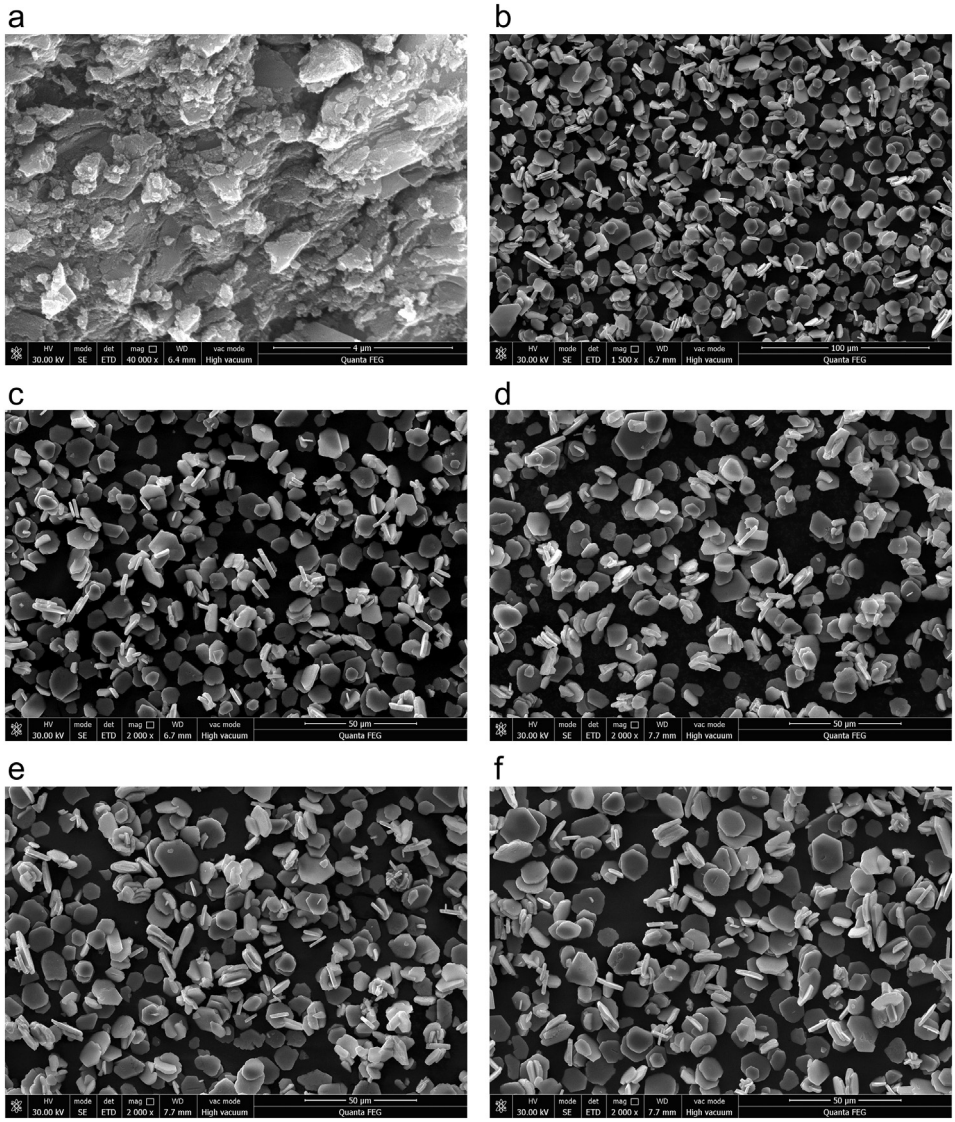

Fig. 6. SEM images of MIO synthesized at different reaction temperatures: (a) 160 °C; (b) 180 °C; (c) 200 °C; (d) 220 °C; (e) 240 °C; (f) 260 °C.

Fig. 7. Physical photo of MIO obtained under the optimized conditions.

iron oxide, and as-synthesized sodium ferrate is easy to hydrolyze [29]. The reactions can be expressed as follows:

$$Fe_2O_3 + Na_2CO_3 \rightarrow 2NaFeO_2 + CO_2 \quad (1)$$

$$FeO_2^- + 2H_2O \rightarrow Fe_2O_3 \cdot H_2O + 2OH^- \quad (2)$$

In view of the above, the gradual disappearance of α-Fe_2O_3 and the reappearance of FeOOH with increased NaOH concentration may be due to the reaction between newly formed α-Fe_2O_3 and sodium hydroxide. In extreme alkaline environment, Fe_2O_3 may react with NaOH to form $NaFeO_2$, which lead to gradual disappearance of Fe_2O_3 diffraction peaks with increased NaOH concentration. In separation and cleaning process of hydrothermal products, $NaFeO_2$ may be hydrolyzed, producing FeOOH. The reactions can be expressed as follows:

$$Fe_2O_3 + 2NaOH \rightarrow 2NaFeO_2 + H_2O \quad (3)$$

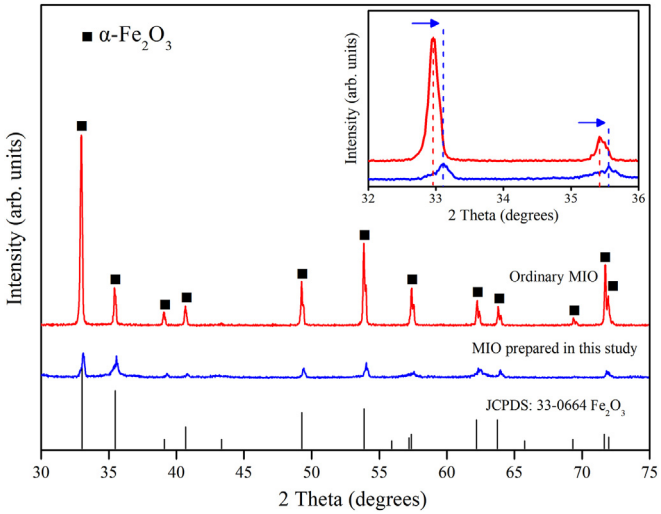

Fig. 8. XRD patterns of ordinary MIO and MIO prepared in this study.

$$FeO_2^- + H_2O \rightarrow FeOOH + OH^- \quad (4)$$

It was noteworthy that, under the same or similar conditions, NaOH concentration required to obtain single phase α-Fe_2O_3 powder in this study was much higher than those reported in previous studies. Zheng et al. reported the synthesis of MIO from pyrite cinders via hydrothermal method [21]. According to their results, the single phase α-Fe_2O_3 powders was achieved at NaOH concentration 1 mol/L, which was only equivalent to 1/14 of the value of this study. This may be due to the difference on the chromium content of the two wastes. Cr/Fe molar ratio of ICGW in this study reaches 2.60×10^{-2}, which is >140 times higher than that of pyrite cinders reported in Zheng's study. The precipitation pH value intervals of iron and chromium are similar. So, chromium will inevitably enter the hydrothermal precursor. According to the data of Krehula et al. [35], Cr can be doped into goethite crystal lattice in highly alkaline media. Moreover, it has been reported that Cr inclusions into iron oxides can improve their corrosion resistance [37]. It can be concluded that incorporation of Cr into goethite crystal lattice strongly stabilized goethite against NaOH dissolution. Therefore, in this study, higher NaOH concentration was required to promote the conversion of goethite to iron oxide.

The SEM micrographs of the products at different NaOH concentration were shown in Fig. 4. From Fig. 4(a), the 4 mol/L sample exhibited needlelike and serious agglomeration, indicating that hydroxide precursor could hardly be transferred to α-Fe_2O_3. This result was consistent with the XRD analysis. With increasing NaOH concentration, the morphology of as-synthesized products changed from needlelike to platelet, and then to flake. Moreover, particle size of the products increased with the increase of NaOH concentration. It may be attributed to increasing NaOH concentration accelerating the nucleation and growth of the α-Fe_2O_3 phase. On the other hand, different morphology of obtained products may be caused by the selective absorption of OH^- groups on a special crystallographic plane, which was consistent with Peng's results [38]. Therefore, the optimal NaOH concentration should be 14 mol/L. Under this condition, the obtained MIO was flaky particle with good crystalline form.

3.2. Hydrothermal temperature

A series of experiments were performed with hydrothermal temperature ranging from 160 °C to 260 °C, while NaOH concentration was fixed at 14 mol/L. Fig. 5 showed the XRD patterns of the products obtained at different hydrothermal temperatures. Table 2 summarized the percentage of the formed phases and its crystalline size. Below 200 °C, samples had a large amount of FeOOH phase. However, samples had almost pure corundum α-Fe_2O_3 structure when the hydrothermal temperature was higher than 200 °C. When the hydrothermal temperature rose from 200 °C to 260 °C, the α-Fe_2O_3 phase content of the corresponding sample increased from 98.2% to 98.8%. In addition, the crystalline size of α-Fe_2O_3 also increased with the increase of hydrothermal temperature. Therefore, hydrothermal temperature played an important role in the formation of α-Fe_2O_3 crystals, and higher temperature aided ferric hydroxide precursor transfer to α-Fe_2O_3.

Fig. 6 presented SEM micrographs of products obtained at different hydrothermal temperatures. From Fig. 6(a), products synthesized at 160 °C exhibited amorphous and serious agglomeration, indicating that ferric hydroxide precursor could not be transferred

Table 3
Unit cell parameters of the α-Fe_2O_3 phase.

Sample	*a* (Å)	*b* (Å)	*c* (Å)
Ordinary MIO	5.036	5.036	13.751
MIO prepared in this study	5.034	5.034	13.738
JCPDS File 33-0664	5.036	5.036	13.749

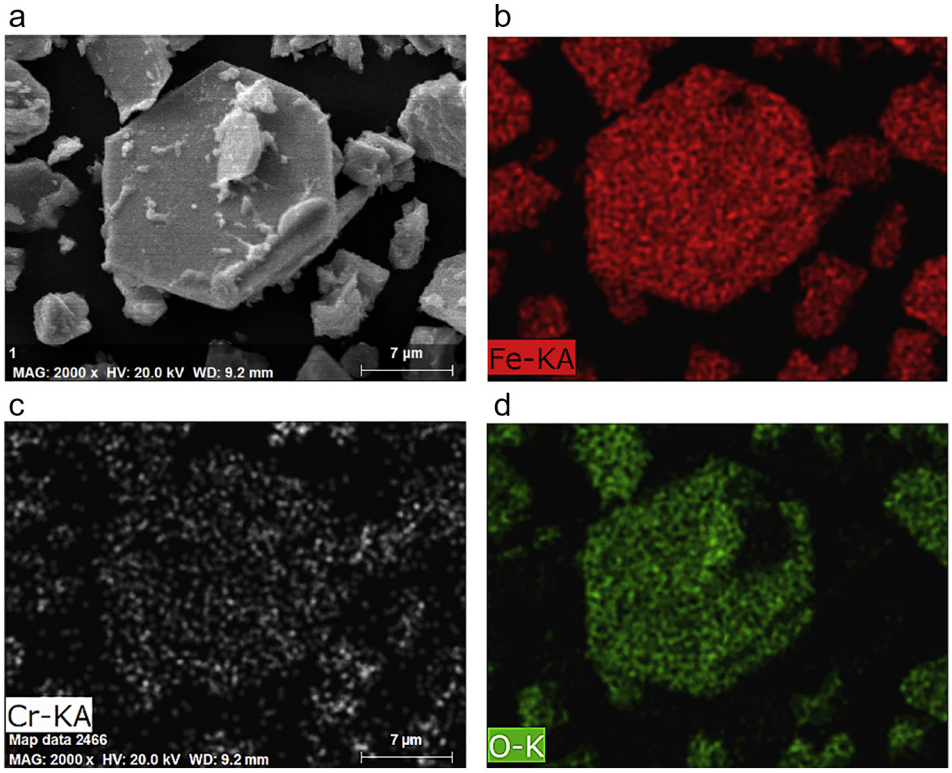

Fig. 9. Maps of iron, chromium and oxygen of MIO prepared in this study.

to α-Fe_2O_3 completely at 160 °C. This result was consistent with the XRD analysis. When the temperature rose to 180 °C, the amount of amorphous powder in the product was greatly reduced. When reaction temperature was higher than 200 °C, the obtained products were uniform flakes and their particle size increased with the reaction temperature. Taking into accounts all these results, along with the economic factors, the optimal hydrothermal reaction temperature was 200 °C.

3.3. Properties of synthesized MIO

To sum up the above discussion, without considering multi-factor coupling actions, the optimized conditions were: sodium hydroxide concentration, 14 mol/L; reaction temperature, 200 °C. The physical photo of the MIO obtained under the optimized conditions was shown in Fig. 7, from which it can be seen that obtained MIO presented a metallic gray. In order to compare the structure, MIO powders were respectively synthesized using chemical grade ferric chloride ($FeCl_3 \cdot 6H_2O$) and ICGW as raw materials, for samples labeled ordinary MIO and MIO prepared in this study, respectively. Fig. 8 showed the XRD patterns of the two MIO, while experimental conditions were kept consistent: 14 mol/L NaOH concentration, 200 °C, 5 h. Compared with the ordinary MIO, the diffraction peaks of MIO prepared in this study moved towards higher diffraction angles (inset in Fig. 8). The unit cell parameters *a*, *b* and *c* of the two MIO were listed in Table 3. For comparison, the unit cell parameters of α-Fe_2O_3, taken from the JCPDS file 33-0664 were also listed in Table 3. Compared with the JCPDS files and the ordinary MIO, *a*, *b* and *c* parameters of MIO prepared in this study were significantly lower. These results illustrate that Cr has been doped into the iron oxide crystal structure.

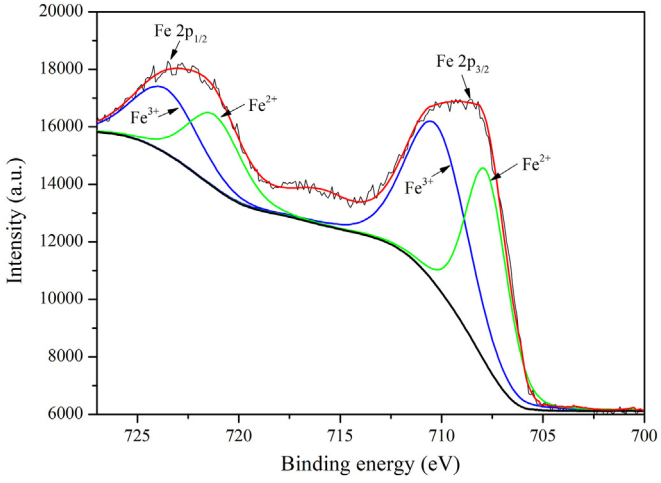

Fig. 10. The XPS spectrum of Fe 2p for the synthesized MIO.

Table 4
The content of oxides of iron in the synthesized MIO powders.

Components	wt%	Components	wt%
Fe_2O_3	97.60	FeO	1.19

Table 5
Quality of MIO synthesized from ICGW under optimal conditions.

Characteristic	ISO 10601-2007 (grade A)	Synthesized sample
Thin-flake content (wt%)	≥65	>85
Iron oxide content (wt%)	≥85	97.60
Oil absorption value (wt%)	13–19	18.20
Matter solubility in water (wt%)	≤0.5	0.40
Matter volatility at 105 °C (wt%)	≤0.5	0.46
pH of aqueous suspension	6–8	7.42
Residue on sieve (wt%)	≤5 (63 μm); ≤0.1 (105 μm)	0

Fig. 9 showed SEM and EDS images of MIO prepared in this study. It was observed from Fig. 9 that the hexagonal flaky particles were obtained, and Cr, Fe and O were evenly distributed.

To study the valence of Fe element in the MIO prepared in this study, the XPS spectra of the Fe 2p regions were recorded. As shown in Fig. 10, each $2p_{3/2}$ and $2p_{1/2}$ peaks for Fe can be split into two peaks by Gaussian-Lorentzian curve fitting. The binding energies for Fe^{3+} $2p_{3/2}$ and $2p_{1/2}$ were 711.0 and 724.1 eV, whereas those for Fe^{2+} $2p_{3/2}$ and $2p_{1/2}$ were 708.1 and 721.4 eV, respectively. From the curve fitting, the presence of Fe ions in the synthesized MIO was confirmed, and the mole ratio of Fe^{3+} to Fe^{2+} on the surface of MIO can reach ~2.12, which was slightly higher than the mole ratio of Fe^{3+} to Fe^{2+} in Fe_3O_4. The chemical analysis results of oxides of iron in the MIO prepared in this study were shown in Table 4. It can be calculated that the content of Fe^{3+} and Fe^{2+} were 68.45% and 0.93%, respectively. The presence of a small amount of Fe^{2+} in synthesized MIO may be due to the incomplete oxidation of the acid leaching solution.

Under the optimal parameters, MIO pigments prepared from ICGW were evaluated according to ISO 10601-2007 (the international standards of MIO pigments for paints), and the results were shown in Table 5. The synthesized MIO met the first rank criterion of ISO 10601-2007.

3.4. Formation mechanism of MIO from iron chromium hydroxide precursors

According to the previous studies [32–34], evolution from ferric hydroxide precursor can be divided into two stages: the iron hydroxide precursors first generate FeOOH, then FeOOH dissolves and generates α-Fe_2O_3. The reactions can be expressed as follows:

$$Fe(OH)_3 \rightarrow FeOOH + H_2O \quad (5)$$

$$2FeOOH \rightarrow \alpha - Fe_2O_3 + H_2O \quad (6)$$

Based on these studies, the mechanism of evolution from iron chromium hydroxide precursors to MIO by the hydrothermal reaction was investigated in this study. Fig. 11 illustrates possible formation mechanism of MIO.

The formation of MIO from iron chromium hydroxide precursors can be broadly divided into three principal steps: dissolution of chromic hydroxide, chromium substituted goethite formation and chromium substituted hematite formation. In the initial stage of hydrothermal reaction, chromic hydroxide was dissolved. The reaction of this process can be expressed as:

$$Cr(OH)_3 + NaOH \rightarrow NaCrO_2 + 2H_2O \quad (7)$$

Then, when transformation from ferric hydroxide to goethite phase occurred, the presence of CrO_2^- ions promoted iron substitution by chromium in the crystal structure of generated goethite, which was consistent with Krehula's results [36]. This period was considered to be the formation of chromium substituted goethite. Under appropriate hydrothermal conditions, α-Fe_2O_3 nuclei grew by the deposition of the solute with the dissolution of chromium substituted goethite. Meanwhile, the presence of CrO_2^- ions in the hydrothermal system promoted iron substitution by chromium in the crystal structure of α-Fe_2O_3. This period was considered to be the formation of chromium substituted hematite. Therefore, for the preparation of MIO from iron chromium hydroxide precursors, it was the key to ensure goethite transformation without destroying nascent MIO crystals.

Based on the above discussions, the Cr^{3+} concentration in the iron chromium hydroxide precursors has a great influence on the formation of MIO. The increasing Cr^{3+} concentration in the precursor can result in more CrO_2^- ions produced in the initial period of hydrothermal reaction. Accordingly, in the chromium substituted goethite formation period, the substitution amount of Cr in goethite will change. The changes in the first two periods will eventually affect the formation of chromium substituted hematite. Except for Cr^{3+}, Fe^{2+} concentration in the iron chromium hydroxide precursors may also have some influence on the formation of MIO. Studies have shown that Fe^{2+} in ferric hydroxide precursor can accelerate the transformation of $Fe(OH)_3$ and promote the formation of hematite particles [22]. In view of this, in this study, the presence of a small amount of Fe^{2+} in the iron chromium hydroxide precursors may be beneficial to the formation of MIO.

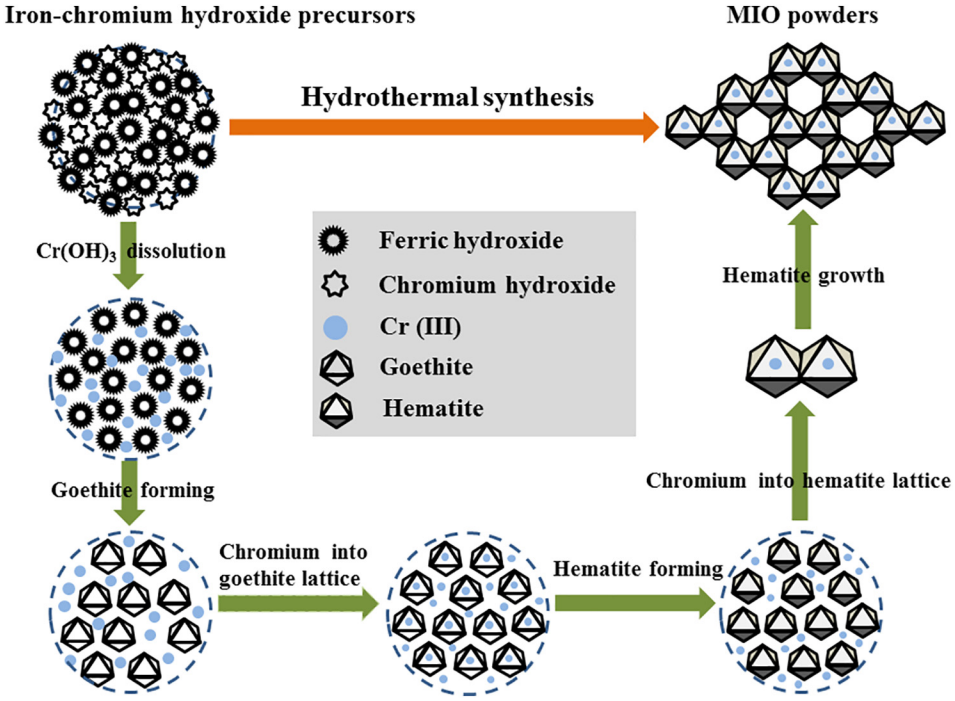

Fig. 11. Possible formation mechanism of MIO from iron chromium hydroxide precursors.

4. Conclusions

Using iron chromium hydroxide precursors obtained from the wet treatment of ICGW as raw materials, MIO pigments were successfully prepared via hydrothermal method. Synthesized MIO powders have high purity (97.6%), even distribution of sizes (~15 μm) and uniform flake. Quality test results showed that synthesized MIO met the first rank criterion of ISO 10601-2007 (the standards of MIO pigments for paints). For the preparation of MIO from iron chromium hydroxide precursors, it was the key to adjust the hydrothermal reaction conditions to ensure goethite transformation without destroying nascent MIO crystals.

Acknowledgements

This work is supported by the National Natural Science Foundation of China (Grant No. 51502014, 51672024 and 51472030) and the Fundamental Research Funds for the Central Universities (Grant No: FRF-IC-17-005). The authors would like to thank the editor for editing of the manuscript and the anonymous reviewers for their detailed and helpful comments.

References

[1] G. Tian, W. Wang, B. Mu, Q. Wang, A. Wang, Cost-efficient, vivid and stable red hybrid pigments derived from naturally available sepiolite and halloysite, Ceram. Int. 43 (2017) 1862–1869.
[2] G.T.W. Wang, D. Wang, Q. Wang, A. Wang, Novel environment friendly inorganic red pigments based on attapulgite, Powder Technol. 315 (2017) 60–67.
[3] J.C. Villalba, V.R.L. Constantino, F.J. Anaissi, Iron oxyhydroxide nanostructured in montmorillonite clays: preparation and characterization, J. Colloid Interface Sci. 349 (2010) 49–55.
[4] F. Franco, M. Benitez-Guerrero, I. Gonzalez-Trivino, R. Perez-Recuerda, C. Assiego, J. Cifuentes-Melchor, J. Pascual-Cosp, Low-cost aluminum and iron oxides supported on dioctahedral and trioctahedral smectites: a comparative study of the effectiveness on the heavy metal adsorption from water, Appl. Clay Sci. 119 (2016) 311–332.
[5] J. Cervini-Silva, A.N. Camacho, E. Palacios, P.D. Angel, M. Pentrak, L. Pentrakova, S. Kaufhold, K. Ufer, M.T. Ramirez-Apan, V. Gomez-Vidales, D.R. Montano, A. Montoya, J.W. Stucki, B.K.G. Theng, Anti-inflammatory, antibacterial, and cytotoxic activity by natural matrices of nano-iron (hydr) oxide/halloysite, Appl. Clay Sci. 120 (2016) 101–110.
[6] Q. Dou, K.M. Ng, Synthesis of various metal stearates and the corresponding monodisperse metal oxide nanoparticles, Powder Technol. 301 (2016) 949–958.
[7] M.N. Kakaei, I. Danaee, Evaluation of cathodic protection behavior of waterborne inorganic zinc-rich silicates containing various contents of MIO pigments, Anti-Corros. Methods Mater. 60 (1) (2013) 37–44.
[8] M. Tamboura, A.M. Mikhailova, M.Q. Jia, Development of heat-resistant anticorrosion urethane siloxane paints, J. Coat. Technol. Res. 10 (3) (2013) 381–396.
[9] H.Q. Yang, Q. Zhang, S.S. Tu, Y. Wang, Y.M. Li, Y. Huang, A study on effects of elastic stress on protective properties of marine coatings on mild steel in artificial seawater, Prog. Org. Coat. 99 (2016) 61–71.
[10] M. Echeverria, C.M. Abrea, K. Lau, C.A. Echeverria, Viability of epoxy-siloxane hybrid coatings for preventing steel corrosion, Prog. Org. Coat. 92 (2016) 29–43.
[11] M. Tamboura, A.M. Mikhailova, M.Q. Jia, A comparative study of anticorrosion paints based on silicone-urethane binders: a multilayer primer, SILICON 6 (2014) 45–56.
[12] H.A. Mohamed, Eco-friendly zero Voc anticorrosive paints for steel protection, J. Appl. Polym. Sci. 125 (2012) 1790–1795.
[13] B. Nikravesh, B. Ramezanzadeh, A.A. Sarabi, S.M. Kasiriha, Evaluation of the corrosion resistance of an epoxy-polyamide coating containing different ratios of micaceous iron oxide/Al pigments, Corros. Sci. 53 (2011) 1592–1603.
[14] E. Langer, H. Kuczynska, E. Kaminska-Tarnawska, J. Lukaszczyk, Self-stratifying coatings containing barrier and active anticorrosive pigments, Prog. Org. Coat. 71 (2011) 162–166.
[15] Y. Haiming, W.M. Cheng, L.R. Wu, H. Wang, Y. Xie, Mechanisms of dust diffuse pollution under forced-exhaust ventilation in fully-mechanized excavation of faces by CFD-DEM, Powder Technol. 317 (2017) 31–47.
[16] Q. Xiao, Y. Sun, J. Zhang, Q.J. Li, Size-dependent of chromium (VI) adsorption on nano α-Fe_2O_3 surface, Appl. Surf. Sci. 356 (2015) 18–23.
[17] C. Tze, United States Patent, Appl.3864463, 1975.
[18] M. Muller, J.C. Villalba, F.Q. Mariani, M. Dalpasquale, M.Z. Lemos, M.F.G. Huila, F.J. Anaissi, Synthesis and characterization of iron oxide pigments through the method of the forced hydrolysis of inorganic salts, Dyes Pigments 120 (2015) 271–278.
[19] S. Krehula, S. Music, The effect of iridium(III) ions on the formation of iron oxides in a highly alkaline medium, J. Alloys Compd. 516 (2012) 207–216.
[20] S. Krehula, G. Setfanic, K. Zadro, L.K. Krehula, M. Marcius, S. Music, Synthesis and properties of iridium-doped hematite (α-Fe_2O_3), J. Alloys Compd. 545 (2012) 200–209.
[21] Y.J. Zheng, Z.C. Liu, Preparation of monodispersed micaceous iron oxide pigment from pyrite cinders, Powder Technol. 207 (2011) 335–342.
[22] Z.C. Liu, Y.J. Zheng, Effect of Fe(II) on the formation of iron oxide synthesized from pyrite cinders by hydrothermal process, Powder Technol. 209 (2011) 119–123.
[23] B. Ruffino, M.C. Zanetti, Recycling of steel from grinding scraps: reclamation plant design and cost analysis, Resour. Conserv. Recycl. 51 (2008) 1315–1321.
[24] L.Z. Shen, Y.S. Qiao, Y. Guo, J.R. Tan, Preparation and formation mechanism of nano-iron oxide black pigment from blast furnace flue dust, Ceram. Int. (1) (2013) 737–744.
[25] S. Wu, A.Z. Sun, F.Q. Zhai, J. W, W.H. Xu, Q. Zhang, A.A. Volinsky, Fe_3O_4 magnetic nanoparticles synthesis from tailings by ultrasonic chemical co-precipitation, Mater. Lett. 65 (2011) 1882–1884.
[26] ISO 787-2, General methods of test for pigments and extenders Part 2, Determination of Matter Volatile at 105 °C, International Organization for Standardization, Switzerland, 1981.
[27] ISO 787-3, General methods of test for pigments and extenders Part 3, Determination of Matter Soluble in Water Hot Extraction Method, International Organization for Standardization, Switzerland, 2000.
[28] ISO 787-5, General methods of test for pigments and extenders Part 5, Determination of Oil Absorption Value, International Organization for Standardization, Switzerland, 1980.
[29] E.N. ISO, 787-9, General Methods of Test for Pigments and Extenders Part 9: Determination of pH Value of an Aqueous Suspension, European Committee for Standardization, Brussels, 1995.
[30] E.N. ISO, 3549, Zinc Dust Pigments for Paints—Specifications and Test Methods, European Committee for Standardization, Brussels, 2002.
[31] B. Liu, S.G. Zhang, D.A. Pan, C.C. Chang, Synthesis and characterization of micaceous iron oxide pigment from oily cold rolling mill sludge, Procedia Environ Sci 31 (2016) 653–661.
[32] T. Otake, D.J. Wesolowski, L.M. Anovitz, L.F. Allard, H. Ohmoto, Mechanisms of iron oxide transformations in hydrothermal systems, Geochim. Cosmochim. Acta 74 (2010) 6141–6156.
[33] S. Das, M. Jim Hendry, J. Essilfie-Dughan, Transformation of two-line ferrihydrite to goethite and hematite as a function of pH and temperature, Environ. Sci. Technol. 45 (2011) 268–275.
[34] T. Sugimoto, S. Waki, H. Itoh, A. Muramatsu, Preparation of monodisperse platelet-type hematite particles from a highly condensed β-FeOOH suspension, Colloids Surf. A Physicochem. Eng. Asp. 109 (1) (1996) 155–165.
[35] X. Li, F. Niu, J. Tan, G. Liu, T. Qi, Z. Peng, Q. Zhou, Removal of S^{2-} ion from sodium aluminate solutions with sodium ferrite, Trans. Nonferrous Metals Soc. China 26 (2016) 1419–1424.
[36] S. Krehula, S. Music, The influence of a Cr-dopant on the properties of α-FeOOH particles precipitated in highly alkaline media, J. Alloys Compd. 469 (1–2) (2009) 336–342.
[37] D.C. Cook, S.J. Oh, R. Balasubramanian, M. Yamashita, The role of goethite in the formation of the protective corrosion layer on steels, Hyperfine Interact. 122 (1–2) (1999) 59–70.
[38] D.F. Peng, S. Beysen, Q. Li, Y.F. Sun, L.Y. Yang, Hydrothermal synthesis of monodisperse α-Fe_2O_3 hexagonal platelets, Particuology 8 (4) (2010) 386–389.